Journal of Mechanical Research and Application (JMRA),Vol. 13 No.4, 1402(2023),24-47

Numerical Simulation of Hollow Spinning Process for Square Cross-Section Cone

Jalil Jamali

(Shoushtar branch- Islamic Azad university- Shoushtar- Iran)

Email: jalil.jamali@iau.ac.ir

a

Abstract

The spinning shaping method simulation and study of relevant parameters such as the amount of force needed for sheet metal forming can be very effective in the improvement of the pieces production and reduction of costs in shaping machine manufacture. The amount of needed force is one of the parameters to consider in shaping the pieces, and it is important to establish a relationship between this parameter and others such as sheet thickness, roller tip diameter and shaping speed. Establishing this relationship will specify the appropriate devices and working conditions during sheets shaping. In this paper, shaping process modeling through the spinning shaping method by explicit dynamic method in ABAQUS software is presented, and the results are compared with available experimental data and Forge 3D software. Therefore, the focus of the present study is an assessment of the effects of working parameters such as, rotation speed, sheet thickness and roller tip radius on shaping spinning process. The results show that the behaviors of shaping process are totally different which indicates the process sensitivity to the working parameters.

Keywords: spinning shaping method, sheet thickness, roller tip diameter, shaping speed, rotation speed

Introduction

Spinning process is an ancient metal forming technology used to manufacture hollow products from metal sheets or tubes [18]. In recent years, extensive experimental and numerical studies have been carried out Spinning process. Xu and Ju [1] investigated the spinning combustion in a mesoscale divergent channel. They found that the spinning flame only occurred after the transition from fast flame regime to slow flame regime. A parameterized toolpath is proposed by Polyblank and Allwood [2] based on a quadratic Bezier curve. Their experimental analysis revealed some new features of process mechanics and leads to a proposal for a set of rules that may become useful for the automatic toolpath generation. The thickness distribution of a spin formed dome in an Aluminum pressure vessel was studied experimentally and a simple formulation to predict the thickness distribution of the dome was proposed by Akkus and Kawahara [3]. The results indicate that the proposed two-step spin forming provides a greater boss thickness than that of conventional forming. A modified process for the dry spinning of carbon nanotube yarn is reported by Tran et al. [4] and then they investigated the effect of heat treatments and other yarn constructions on the tensile properties. Their experimental results show that the tensile properties were significantly improved. Quigleya and Monaghan [5] presented an experimental analysis of the spinning process in which the strains were discussed. Simple experimental shapes have been produced with different diameters of the blanks. An attempt of forming variant wall thickness distributions in the same shape has been investigated; specifically, an oblique sheet spinning process has been used. The wall thickness distribution based on a simple shear deformation model of parts formed at several inclination angles has been discussed [6, 7]. Fundamentals of controlling the thickness and surface quality during dieless necking-in of tubes have been presented by Kwiatkowski and Tekkaya [8]. An experimental analysis of robotic metal spinning has been implemented by Ozer et al. [9]. The experiments have been conducted with enhanced cascaded trajectory tracking algorithms

with an add-on vibration suppressor. Professional spinning manufacturers typically use tools with a single, combined, or multi-pass rollers mounted on a steel-tube handle for forming the products. Akio and Hirohiko [10] tried to control the wall thickness distribution and claimed that the synchronous die-less spinning method is suitable for varying the wall thickness. Wang and Long [11, 12] studied conventional multi-pass shear spinning process and pointed out that the wall thickness of the work piece decreases gradually after each forward roller pass. The investigations above show that the hollow spinning is flexible for many products, and it is an important topic to discuss that the wall thickness distribution is impacted deeply by roller path. Lai and Xia et al. [13] investigated the spinning process of the hollow cone with triangular cross-section and revealed its stress and strain distributions. Shimizu [14] derived the roller path for elliptical cone formed by synchronous spinning. The effects of roller paths on dimensional precision in die-less spinning of sheet metal have examined numerically by Li et al. [15]. Liu et al. [16] studied the stress and strain distributions of first-pass conventional spinning under different roller-traces with an Elasto-plastic FEM method. Hwang et al [17] Numerically Investigated the Effect of Process Parameters during Aluminium Wheel Flow-Forming. Zeng et al. [19] established a 3D finite element model to investigate on the spinnability of the ellipsoidal power spinning. The results show that the equivalent stress and the equivalent plastic strain increase with the forming time. Furthermore, they confirmed the Johnson–Cook fracture criterion during the ellipsoidal power spinning. An Elasto-plastic incremental finite-element computer program has been developed to simulate the forming process by Kemin et al [20] in order to be able to gain understanding of the characteristics of tube spinning theoretically. Song et al [21] examined the phenomenon of diametric growth in the forward flow forming process through finite element simulation and experimental investigation.

By Cha et al. [22], the mechanism of the backflow is studied as well as the process conditions to prevent backflow by establishing a numerical analysis procedure using SHAPE-RR FEM program. Effects of processing parameters on the surface quality of the square section die-less spinning investigated by Jia et al. [23].

Indeed, very little is known about the effect of working parameters on the shaping spinning process. Due to immense applications of this process in the various important practical processes, this technology requires further investigations to understand the behaviors under different working parameters. In the present study, the shaping spinning process is numerically examined by explicit dynamic method in ABAQUS software for various effective parameters. The obtained results are compared with the published experimental measurements [24] to ensure the numerical method. The special feature of this study is that here is considered the effect of rotation speed, sheet thickness and roller tip radius on shaping spinning process.

2- Geometrical Model

In the present work, the Al99 sheet with several thickness of 1, 2, and 3 mm as well as the roller with tip diameters of 2, 4, and 6 mm are considered, which show in Figs. 1 and 2, schematically. It should be note that, in order to compared the current numerical results with experimental data [24] the aluminum sheet thickness and the tip's diameters are achieved 1 and 2 mm, respectively. Furthermore, Fig. 3 shows that the roller's position relative to the aluminum sheet with an angle of 45^{o}, according to the experimental conditions [24].

The chemical compounds are tabulated in Table 1, according to the data from Jia et al. [24]. The performed analysis is dynamic and deformation speed is high; therefore, strain rate values must be taken into account in the simulation. Material’s plastic behavior is considered to be dependent on the strain rate and the stress-strain diagram is shown in Fig. 4, for different strain rates based on Eq. (4). The data in this figure are derived based on Eq. (1).

$$\sigma_f = Ae^{(m_1 T)} T^{m9} \varepsilon^{m2} e^{m4/\varepsilon} (1+\varepsilon)^{m5T} e^{m7\varepsilon} \dot{\varepsilon}^{m3} \dot{\varepsilon}^{m8T} \quad (1)$$

In this equation, σ_f , T, ε and $\dot{\varepsilon}$ are stress, temperature, strain and strain rate in inverse seconds, respectively, as well as A, m1, m2, m3, m4, m5, m7, m8, m9 are all constant values brought in Table 2.

Solving Method

To solve the problem, the explicit dynamic method is employed in ABAQUS software. This method is appropriate for simulation of problems in which there exists lots of deformations and complex contacts between pieces where the rate of convergence of results is improved. Nonlinear equations of mechanics of materials are employed, i.e. large deformations were accounted for.

For problem simulation, the sheet remains still and the roller traverses the specified area and forms the sheet; hence, the roller's movement should be defined by mathematical relations. As shown in Fig. 5, if the roller is moved from A to B, the relationship between roller's rotation radius (r) and cylinder's rotation angle (θ) can be determined in cylindrical coordinates. The relationship between the roller's rotation radius and the rotation angle are brought in Eqs. 2 and 3. Note that moving from A to B radially, there is a change of Δr in the moving direction; and this change in radius is equivalent to a Δθ rotation. The overall roller rotation is designated by θ. The initial roller radius is r_0, and r_{t1} and r_{t2} represent the radial location of A and B. θ_x is movement in radius direction and θ_q is half of the path's corner angles. Boundary conditions in ABAQUS are defined in Cartesian coordinates; therefore, so should be defined the roller's way of movement. Roller path in Cartesian coordinates is performed through conversion of coordinate systems and MATLAB programming. The roller path derived from MATLAB codes is shown in Fig. 6. As illustrated, the roller rotates 15 times to create a depth of 16 mm.

$$\theta_x = \arctan\left(\frac{\Delta r}{(r_0 \Delta r)\tan(45-\theta_q)}\right) \quad (2)$$

$$r_t = \frac{r_0 Cos(\theta_x)}{Cos(\theta_x - \theta_1)} \quad (3)$$

Roller position in X, Y and Z directions is determined by the code as time dependent, which is shown in Fig. 7 (a-c) for a roller rotation of 30 RPM. In this project three speeds (30, 50 and 70) are simulated and the results are studied. Point by point derivatives of position data and velocity values in each direction have been calculated in order to exert the proper movement on the roller.

The central part of the aluminum sheet; that is placed in the shaping machine, has been constrained in every direction. In Fig. 8, the location of these boundary conditions is shown. Friction coefficient between the roller and the sheet is considered to be 0.1 and the normal contact properties are defined as hard contact. In addition, the hardness coefficient between the two objects is increased to the extent as not to impinge on convergence, making minimum the influence of objects on each other. It should be noted that while investigating the effect of speed, thickness and roller' tip radius, a tensile force of 10000 $N.m^{-1}$ is exerted on the sheet trailing edge so as to prevent distortions. This force prevents deformation of the sheet trailing edge.

GRID

Figure 9 displays the schematic of aluminum sheet with linear and quadratic tetrahedral elements. Four computing nodes are used, which are represented with the acronym S4R which is appropriate for grid generation of either thin or thick shells. The number of elements is equal to 11000 and according to the Fig. 9, for a reduction in calculation time, bigger sized elements are employed for the region outside the shaping field.

Results and Discussion

Validation

Fig. 10 illustrates the final shape of the piece from three methods; namely simulation in ABAQUS, Forge 3D software [24] and experimental method [24]. The similarity between the overall schematic of the simulated piece in ABAQUS with the experimental method is evident in this figure. Also, in Table 3, different parameters are calculated and compared in the three methods such as the initial radius of the final model, its depth and piece's length. As is evident from the data brought in Table 3 and root of R-square [25-27] values, the method of present simulation has successfully predicted these values with comparison of experimental data [24].

Figure 11 shows the sheet deformation in order to comparison between the current simulation and Forge 3D [24] for the times of 9, 18 and 30 s. Based on presented figures, deformation calculated in both programs at different times are close. Fig. 12 shows the von Mises stress distribution predicted by both programs. Based on the presented contours, difference in maximum stress in the two programs has an acceptable difference of 1.4 percent. In Fig. 13, the predicted plastic strain by both programs and at different times is illustrated, which as well shows matching results.

Figure 14 indicates the sheet thickness after forming at 0, 90, 180 and 270 degree(s) in different locations along the sheet (based on Fig. 1), according to the experiment condition [24] and simulations performed by ABAQUS and Forge 3D [24]. As illustrated in the figures, the thickness obtained in ABAQUS is very close to that found in experiment; hence, ABAQUS software has been successfully able to simulate the shaping process through method of spinning shaping of the aluminum sheet. Higher accuracy of ABAQUSE simulation may be due to the applying the regular grids.

Effect of rotation speed

In this section, we investigated the effects of rotational speed of the roller the necessary force for sheet forming process. In this regard, the tip diameter and sheet thickness are considered to be 4 and 1 mm, respectively, and via three rotational speeds, i.e. 30, 50 and 70 rpm.

Figures 15 and 16 display the vertical and radial forces exerted on the roller depending on time in various roller speeds. These are in fact the forces needed to form a sheet with several roller speed. The radial force is considered as the vector sum of the two horizontal forces as compared to the initial sheet state, and according to the figures, force values are oscillatory. Minimum vertical force is formed in the corners since the roller does not advance there in vertical direction. Vertical force is increased as deformation does which is due to formation of more forces in the sheet. Amount of this force becomes constant after several rotations. Radial force is maximum in the corners as the roller rotation radius there is a lot less than other locations.

Maximum vertical and radial forces exerted on the roller for different rotational speeds are shown in Fig. 17 (a-b), respectively. According to figures, the force exerted on the roller is reduced with increase in rotational speed. Decease in vertical force from 30 to 50 rpm is about 1.3 percent and about 0.3 percent from 50 to 70 rpm. Hence with an increase in speed, the necessary force for sheet forming reduces, yet its effect is not considerable. Also, with an increase in rotational speed, its effect in reducing vertical force decreases. Change in radial force with respect to rotational speed is similar to the vertical force; yet the effect of speed is more considerable. Decrease in radial force from 30 to 50 rpm is about 14 percent.

Effect of sheet thickness

Undoubtedly the more sheet thickness is, the more is the necessary force for sheet forming but the relationship between the two in the spinning method is of importance in selecting conditions and suitable devices. In current analyses, the tip radius is 2mm with a rotational speed of 30 rpm. Three different sheet thicknesses, namely 1, 2 and 3 mm were investigated.

In Figs. 18, the vertical exerted force on the roller for thicknesses 1, 2 and 3 mm is shown respectively. As seen in the figures, for a thickness of 1 mm, maximum force is produced at the end of shaping process. While in the case of the 3 mm thickness, maximum force occurs at the beginning. Furthermore, Fig. 19 shows the radial exerted force on the roller for the three thicknesses during shaping process. The reduction from 50 to 70 rpm is about 5.5 percent.

Maximum vertical and radial forces for the three thicknesses are illustrated in Fig. 20 (a-b). As seen in the figure, the change in force with respect to thickness is not linear and its rate augments with an increase in thickness. Vertical and radial forces experience an increase of 64 and 49%, respectively, as the thickness changes from 1 to 2 mm. a change in thickness from 2 to 3 mm also causes 116 and 214 percent increase in vertical and radial forces, respectively.

Effect of roller tip radius

In order to investigate the tip radius effects on the forces, a shaping process with thickness of 1 mm, rotational speed of 30 RPM with three different roller tip radii, namely 1, 2 and 3 mm is simulated. In Figs. 21 and 22, the vertical and radial forces exerted on the roller over time is illustrated for three tip thicknesses, i.e. 1, 2 and 3 mm, respectively. According to figures, it is evident that the forces exerted on the roller with 3 mm tip radius reaches its maximum at the end of the shaping process while in smaller radial maximum force occurs at the beginning.

In figs. 23 (a-b), the maximum vertical and radial forces for different tip radii are shown. Based on the figures, the maximum force on the roller decreases with an increase in tip radii and its rate of change augments with an increase in thickness. With an increase in the tip radius from 1 to 2 mm, the amount of maximum vertical and radial forces decrease about 0.9

and 5.4, respectively. Their maximum amounts reduce about 0.6 and 16.9 as the tip radius increases from 2 to 3 mm, respectively.

Conclusion

In this paper, the shaping process modeling through the spinning shaping method have been investigated by explicit dynamic method in ABAQUS software, and the results are compared with available experimental data [24] and Forge 3D software [24]. The results show that the predicted results of present work have been compared with experimental data [24] has higher accuracy than Forge 3D [24]. Afterwards, the effects of working parameters such as, rotation speed, sheet thickness and roller tip radius on shaping spinning process. The obtained results are as follows;

- As the rotational roller speed increases, the total force decrease up to 14.1 percent.
- The results indicate that increased force on the roller with thickness have a nonlinear relationship and the forces change rate increases with rising the thickness.
- As the roller tip radius increases, the total forces decrease up to 16.9 percent.

References

1. Xu, B., Ju, Y., 2007. Experimental study of spinning combustion in a mesoscale divergent channel. Proceedings of the Combustion Institute 31, 3285-3292.
2. Polyblank, J.A. & Allwood, J.M. [2015] Parametric toolpath design in metal spinning. *CIRP Annals - Manufacturing Technology*, **64**(1), 301-304.
3. Akkus, N., Kawahara, M., 2006. An experimental and analytical study on dome forming of seamless Al tube by spinning process. Journal of Materials Processing Technology 173, 145-150
4. Tran, C.D., Humphries, W., Smith, S.M., Huynh, C., Lucas, S., 2009. Improving the tensile strength of carbon nanotube spun yarns using a modified spinning process. Carbon 47, 2662-2670
5. Quigley, E., Monaghan, J., 2000. Metal forming: an analysis of spinning processes. Journal of Materials Processing Technology 103, 114-119.

6. Sekiguchi, A., Arai, H., 2012. Control of wall thickness distribution by oblique shear spinning methods. Journal of Materials Processing Technology 212, 786-793.
7. Sekiguchi, A., Arai, H., 2012. Control of wall thickness distribution by oblique shear spinning methods. Journal of Materials Processing Technology 212, 786-793
8. Kwiatkowski, L., Tekkaya, A.E., Kleiner, M., 2013. Fundamentals for controlling thickness and surface quality during dieless necking-in of tubes by spinning. CIRP Annals - Manufacturing Technology 62, 299-302.
9. Özer, A., Sekiguchi, A., Arai, H., 2012. Experimental implementation and analysis of robotic metal spinning with enhanced trajectory tracking algorithms. Robotics and Computer-Integrated Manufacturing 28, 539-550
10. Sekiguchi, A., Arai, H., 2012. Control of wall thickness distribution by oblique shear spinning methods. Journal of Materials Processing Technology 212, 786-793.
11. Wang, L., Long, H., 2013. Roller path design by tool compensation in multi-pass conventional spinning. Materials & Design 46, 645-653.
12. Wang, L., Long, H., 2011. Investigation of material deformation in multi-pass conventional metal spinning. Materials & Design 32, 2891-2899.
13. Xia, Q., Lai, Z., Long, H., Cheng, X., 2013. A study of the spinning force of hollow parts with triangular cross sections. Int J Adv Manuf Technol 68, 2461-2470.
14. Shimizu, I., 2010. Asymmetric forming of aluminum sheets by synchronous spinning. Journal of Materials Processing Technology 210, 585-592.
15. Li, Y., Wang, J., Lu, G.-d. & Pan, G.-j. [2014] A numerical study of the effects of roller paths on dimensional precision in die-less spinning of sheet metal. *Journal of Zhejiang University SCIENCE A*, **15**(6), 432-446
16. Liu, J.H., Yang, H. & Li, Y.Q. [2002] A study of the stress and strain distributions of first-pass conventional spinning under different roller-traces. *Journal of Materials Processing Technology*, **129**(1–3), 326-329
17. Hwang, S.Y., Kim, N. & Lee, C.-s. [2015] Numerical Investigation on the Effect of Process Parameters during Aluminum Wheel Flow-Forming. *Strojniški vestnik-Journal of Mechanical Engineering*, **61**(7-8), 471-476
18. Wong, C.C., Dean, T.A., Lin, J.: A review of spinning, shear forming and flow forming processes. International Journal of Machine Tools and Manufacture **43**(14), 1419-1435 (2003)

19. [Zeng, R., Ma, F., Huang, L. & Li, J. [2015] Investigation on spinnability of profiled power spinning of aluminum alloy. *The International Journal of Advanced Manufacturing Technology*, **80**(1-4), 535-548
20. Kemin, X., Zhen, W., Yan, L. & Kezhi, L. [1997] Elasto-plastic FEM analysis and experimental study of diametral growth in tube spinning. *Journal of Materials Processing Technology*, **69**(1–3), 172-175
21. Song, X., Fong, K.S., Oon, S.R., Tiong, W.R., Li, P.F., Korsunsky, A. & Danno, A. [2014] Diametrical growth in the forward flow forming process: simulation, validation, and prediction. The International Journal of Advanced Manufacturing Technology, 71(1-4), 207-217.
22. Cha, W.-g., Hwang, S., Kim, N. & Lee, C.-s. [2014] Analysis of mechanism of backflow defect of the aluminum wheel flow forming. *International Journal of Precision Engineering and Manufacturing*, **15**(6), 1075-1080
23. Jia, Z., Han, Z.R., Xu, Q., Peng, W.F. & Kong, Q.M. [2015] Effects of processing parameters on the surface quality of square section die-less spinning. *The International Journal of Advanced Manufacturing Technology*, **80**(9-12), 1689-1700.
24. Jia, Z., Han, Z.R., Xu, Q. & Peng, W.F. [2014] Numerical simulation and experimental study on hollow spinning process for square cross-section cone. *The International Journal of Advanced Manufacturing Technology*, **75**(9-12), 1605-1612.
25. Mousavi, S.M. & Roohi, E. [2014] Large eddy simulation of shock train in a convergent–divergent nozzle. *International Journal of Modern Physics C*, **25**(04), 1450003.
26. Mousavi, S.M. & Roohi, E. [2014] Three dimensional investigation of the shock train structure in a convergent–divergent nozzle. *Acta Astronautica*, **105**(1), 117-127.
27. Mousavi, S. & Abolfazli-Esfahani, J. [2014] Numerical investigation of the flameless oxidation of natural gas in the IFRF furnace using large eddy simulation. *International Journal of Spray and Combustion Dynamics*, **6**(4), 387-410.

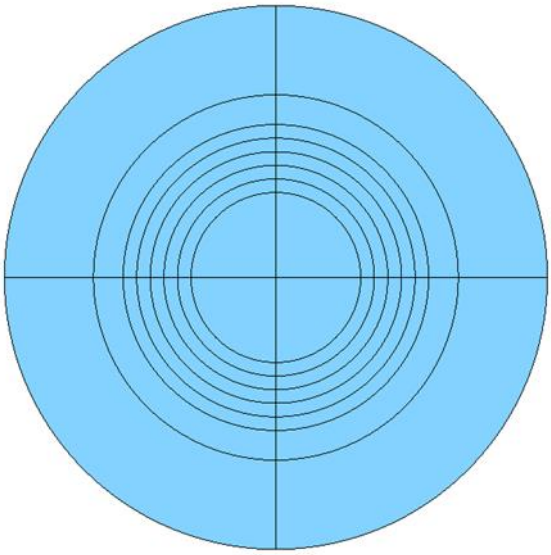

R=80 mm

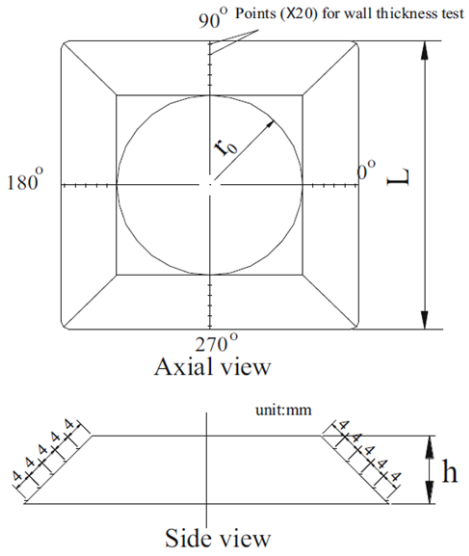

r_0=25 mm, L=77.7 mm, h=16 mm

Figure 1. Model geometry and dimensions of the aluminum plate before and after forming

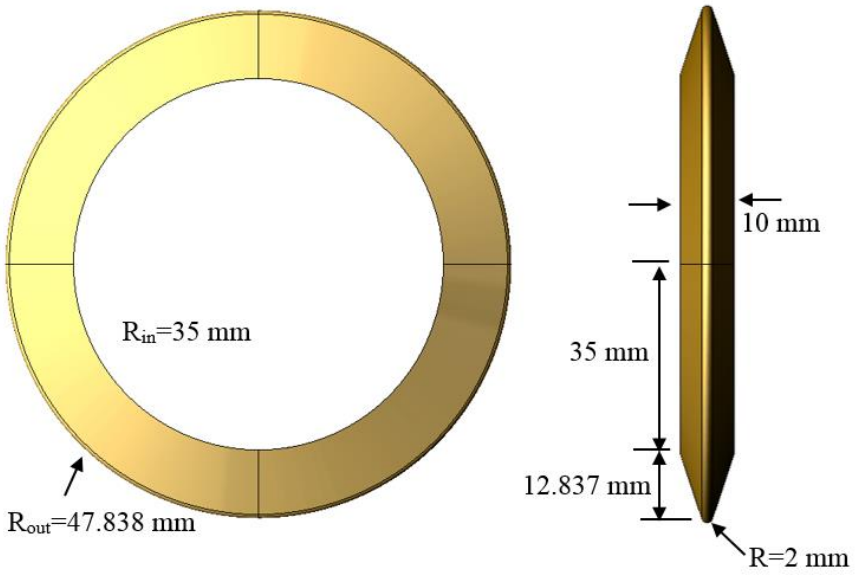

Figure 2. Roller geometrical model and dimensions

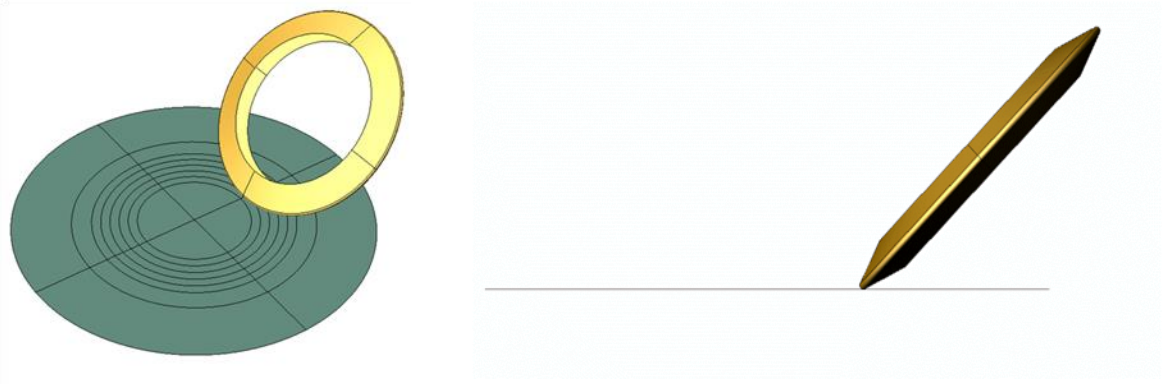

Figure 3. placement of aluminum sheet and roller

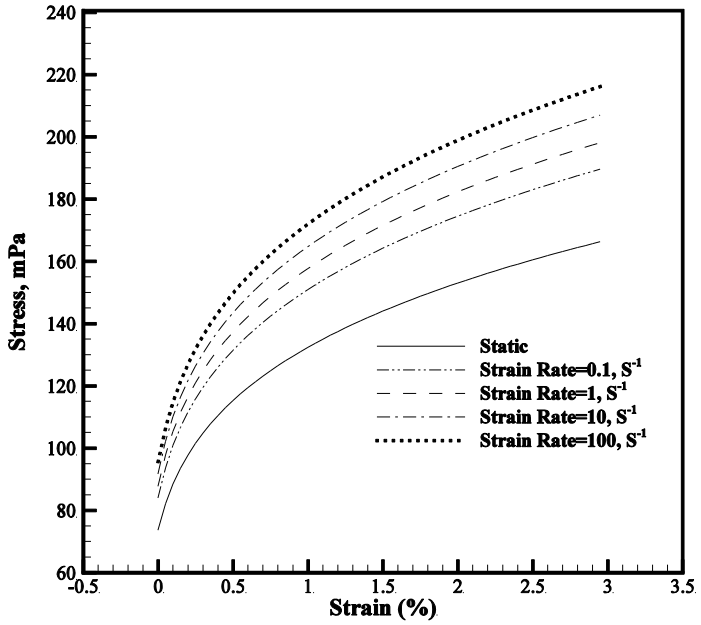

Figure 4: stress-strain diagram of A99 for different strain rates [1]

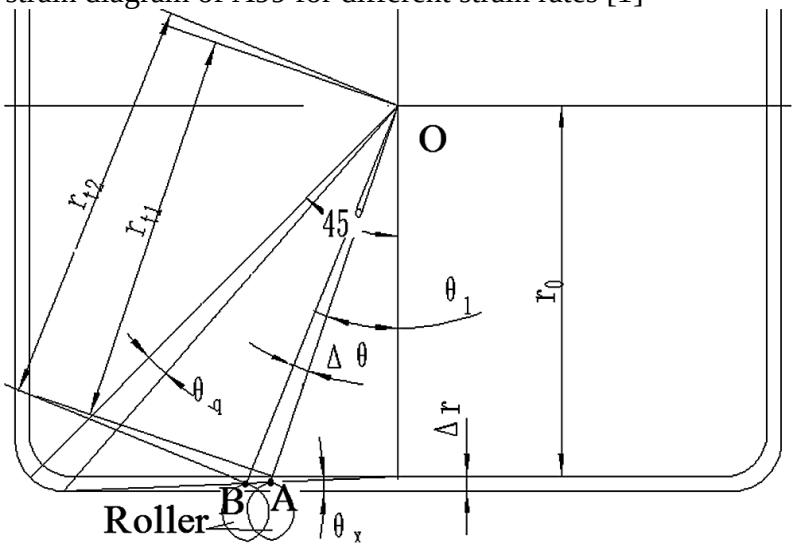

Figure 5: Location of roller in one rotation

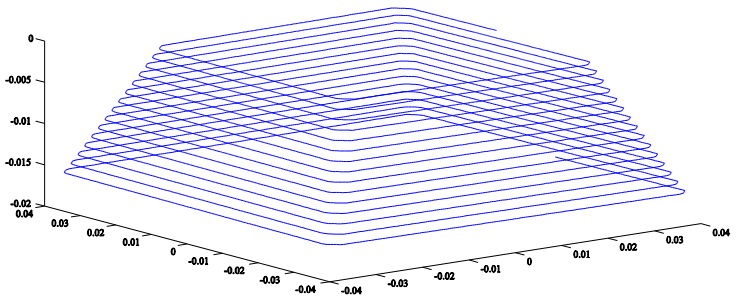

Figure 6: Roller path calculated by the MATLAB code

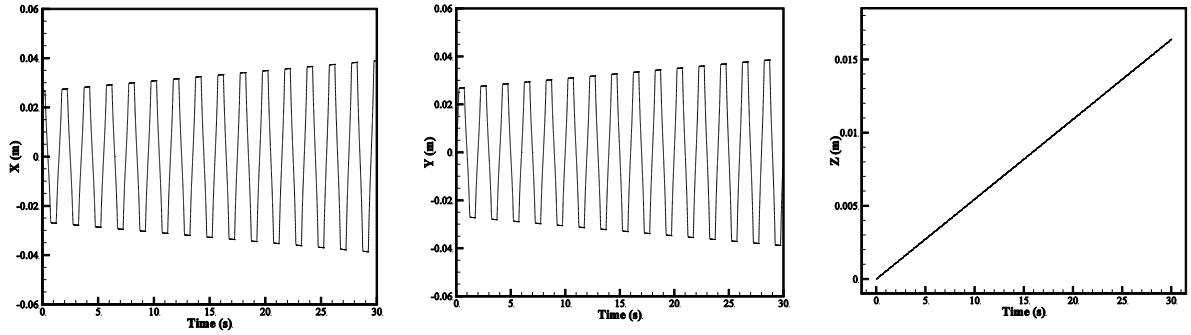

X-Coordinate Y-Coordinate Z-Coordinate

Figure 7: Roller position during analysis

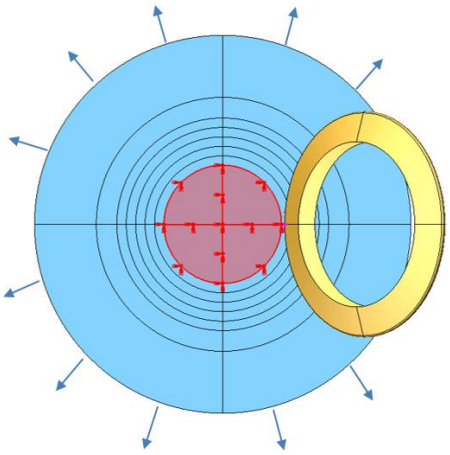

Figure 8: Place of aluminum foil which is bound on all sides

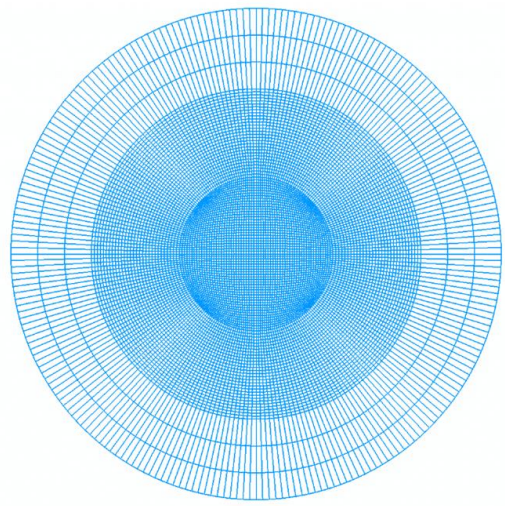

Figure 9: schematic of aluminum sheet Grid

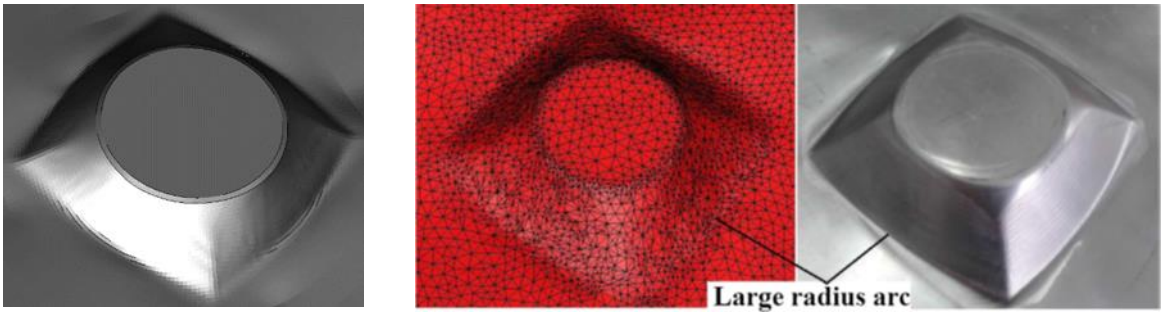

ABAQUS Simulation Forge3D Simulation Experimental

Figure 10: Final shape of obtained piece

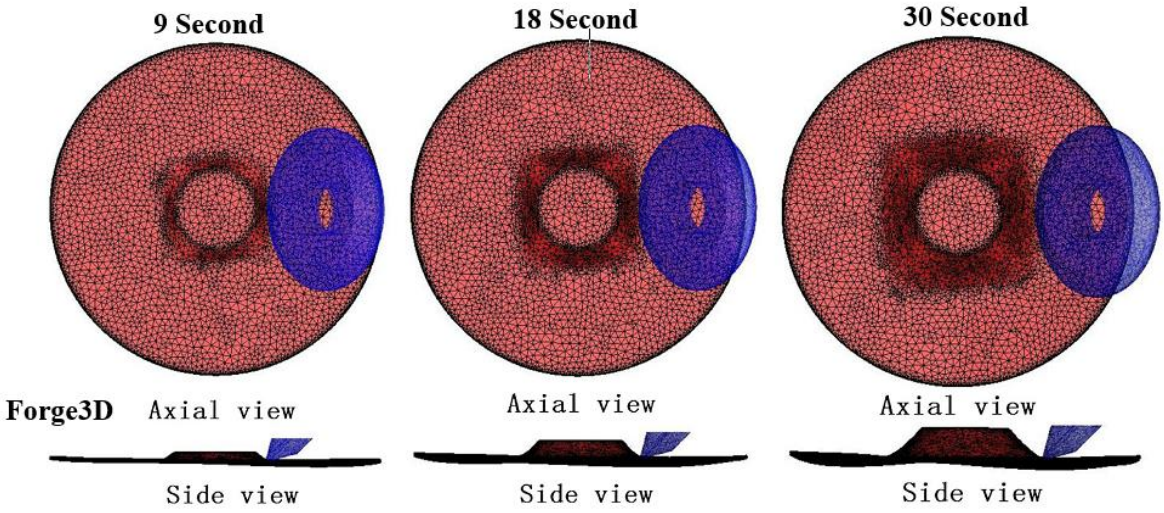

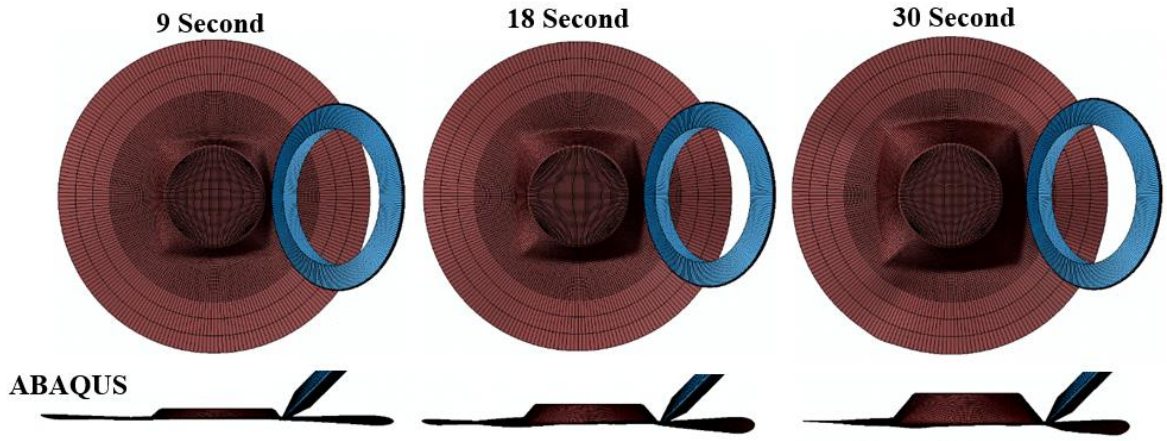

Figure 11: Sheet deformation in 9, 13 and 30 seconds after the commencement of analysis in both ABAQUS and Forge 3D [19]

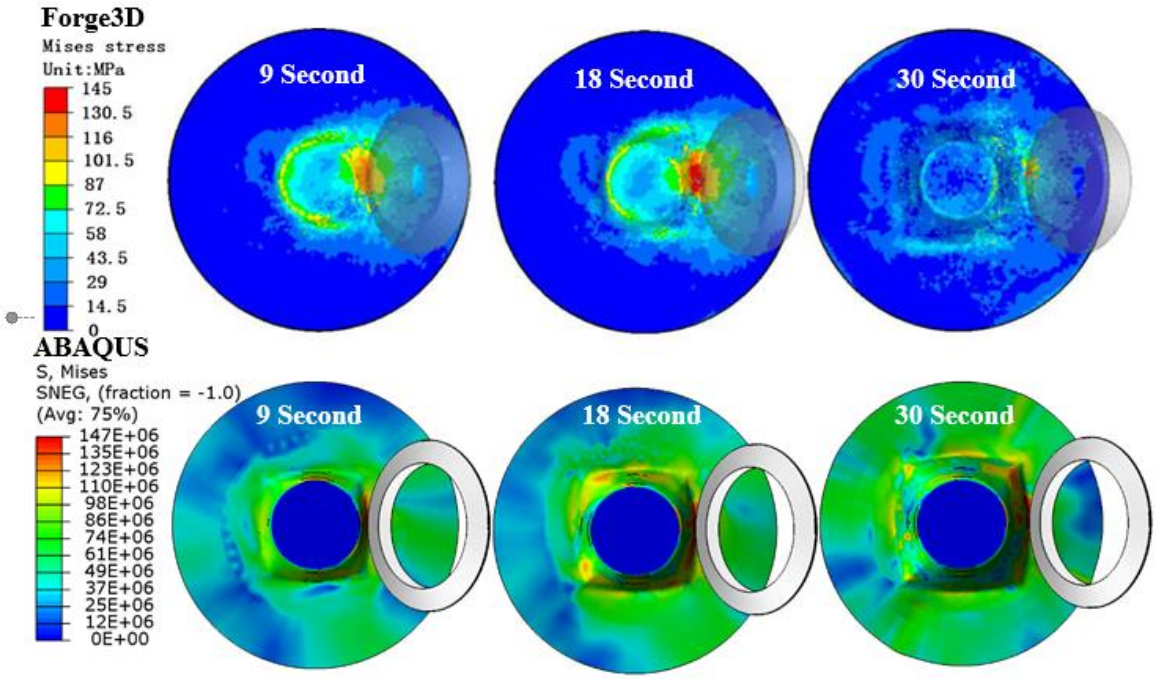

Figure 12: von Mises stress distribution predicted by both ABAQUS and Forge 3D [19]

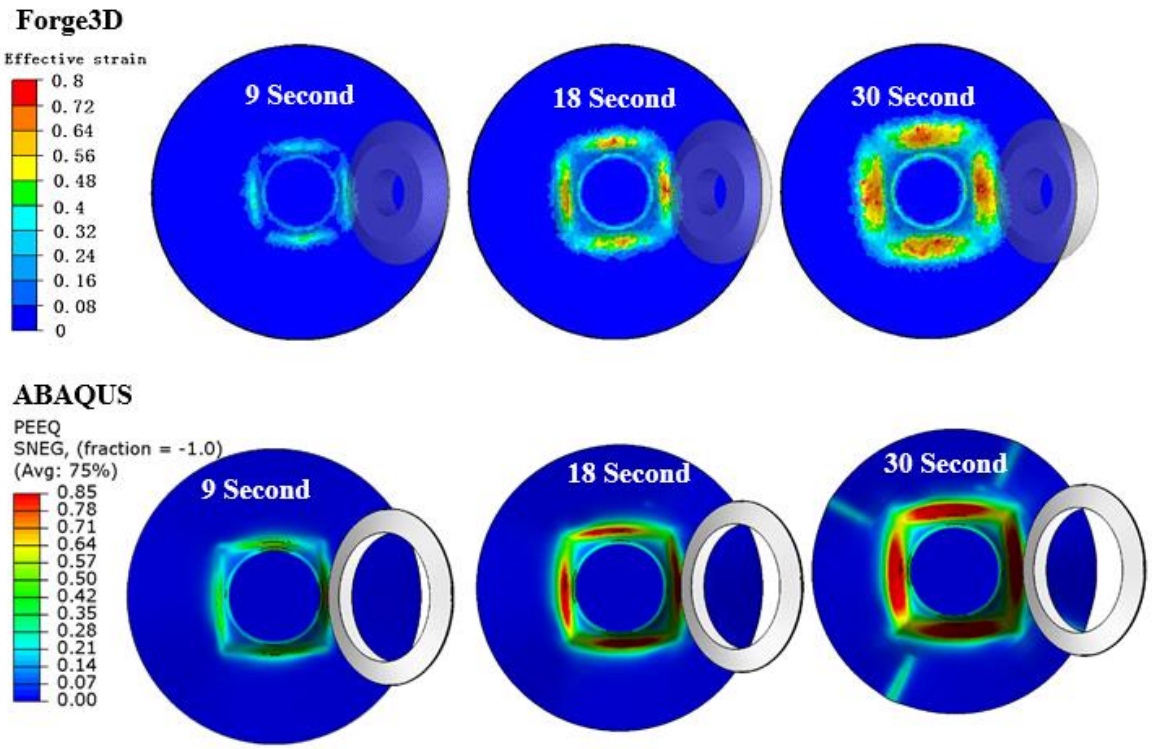

Figure 13: predicted plastic strain by both ABAQUS and Forge 3D [19] and at different times

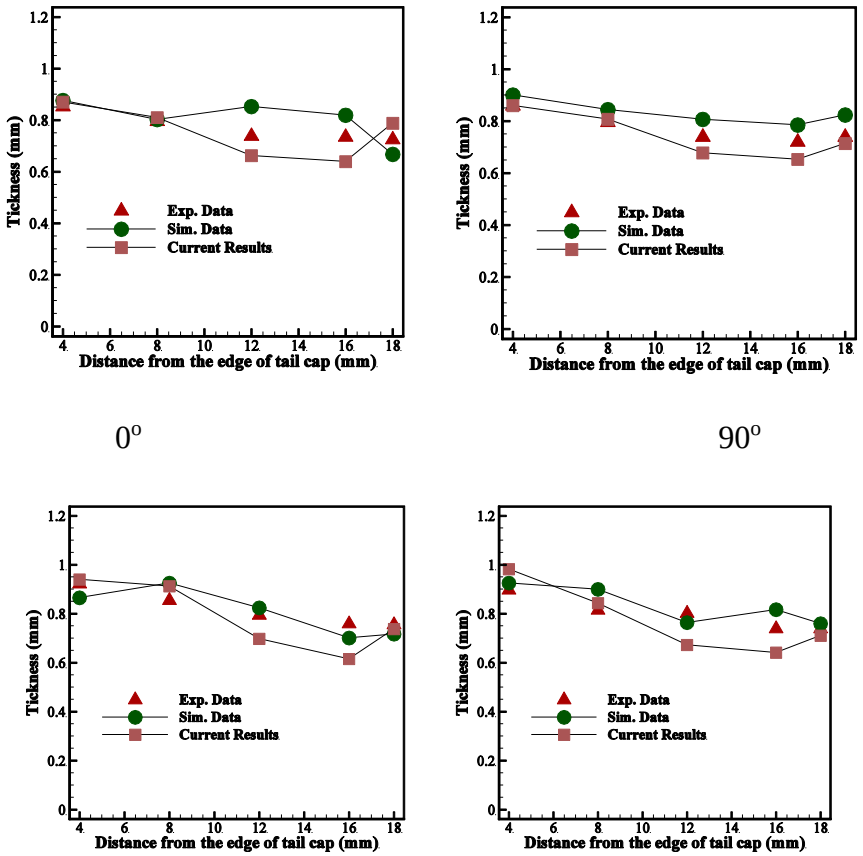

180º 270º

Figure 14: Thickness of the sheet after shaping

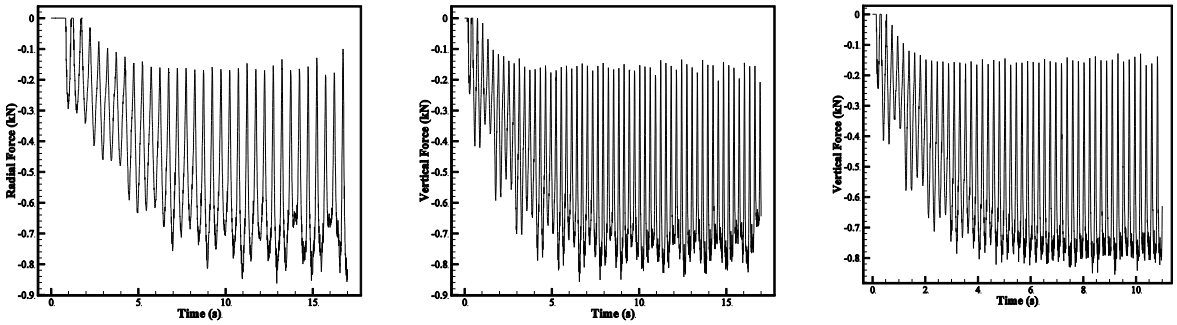

Figure 15: Vertical force exerted on the roller in shaping during

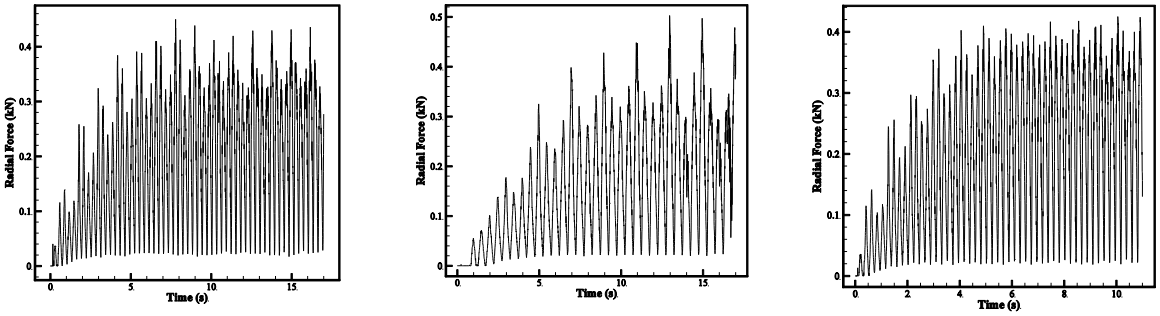

Figure 16: Radial force exerted on the roller in shaping during

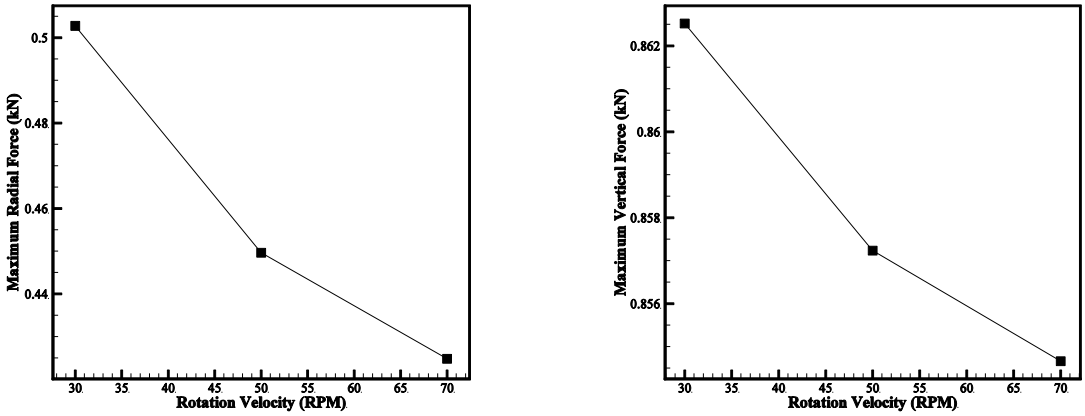

a- vertical b- Radial

Figure 17: Maximum a- vertical and b- radial force exerted on the roller for different rotational speeds

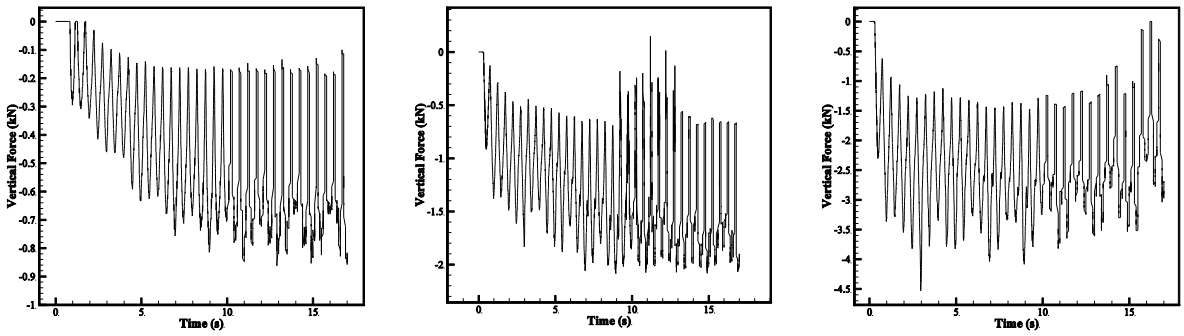

a- 1mm b- 2mm 3mm

Figure 18: Vertical force exerted on the roller for a sheet thickness of a- 1 mm, b- 2mm and c- 3mm during shaping

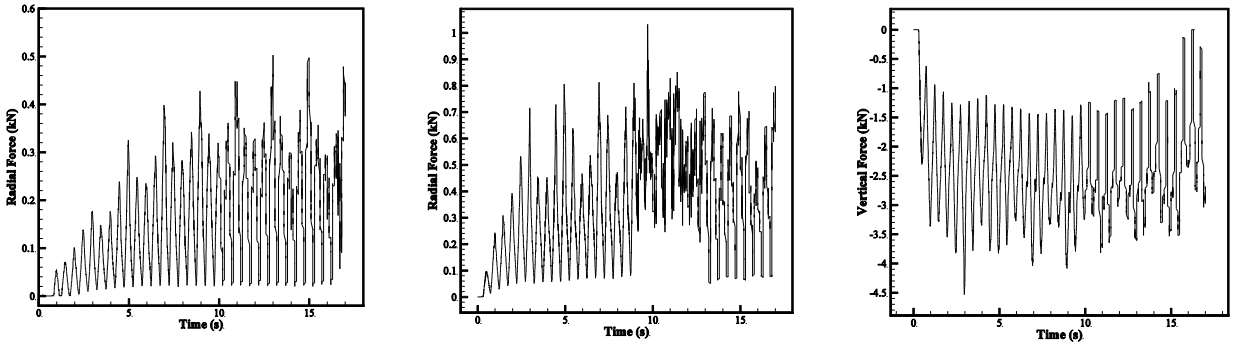

a- 1mm b- 2mm c- 3mm

Figure 19: Radial force exerted on the roller for a sheet thickness of a- 1 mm, b- 2mm and c- 3mm during shaping

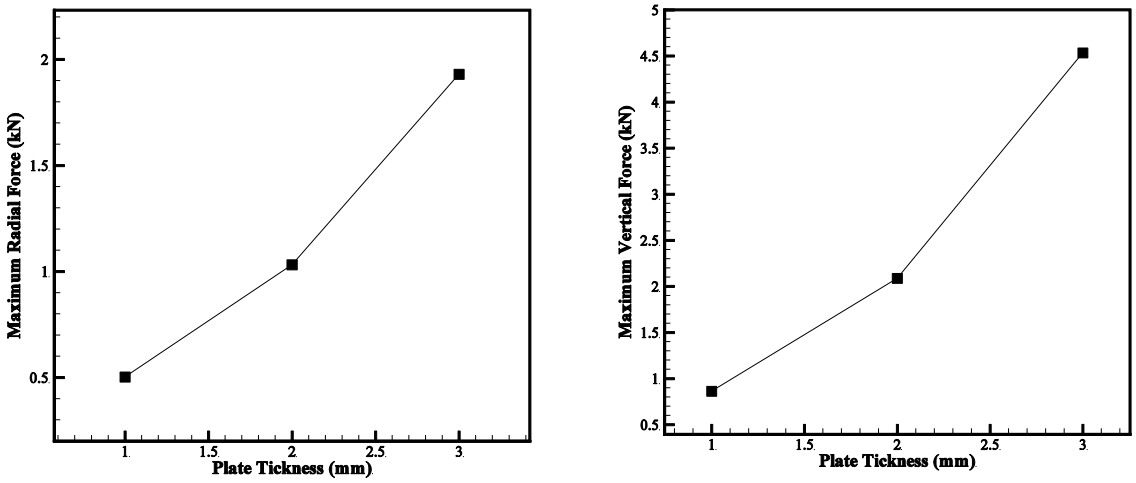

a- Vertical b- Radial

Figure 20: Maximum a- vertical and b- radial forces exerted on the roller for different thicknesses

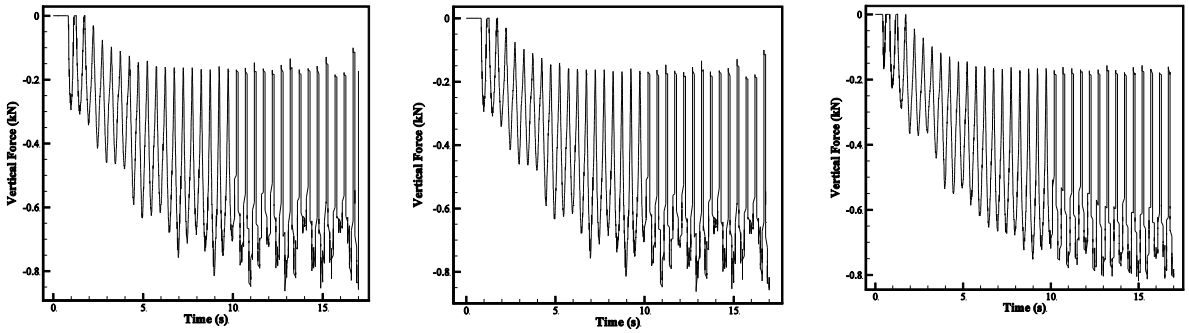

a- 1mm d- 2mm c- 3mm

Figure 21: Vertical force exerted on the roller at the during of sheets shaping for a radius of a- 1 mm, b- 2 mm and c-3 mm tip roller

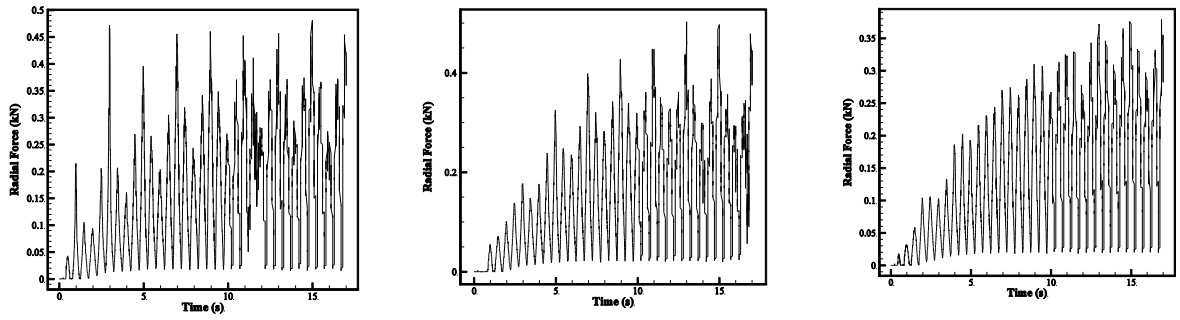

a- 1mm b- 2mm c- 3mm

Figure 22: Radial force exerted on the roller at the during of sheets shaping for a radius of a- 1 mm, b- 2mm and c-3 mm tip roller

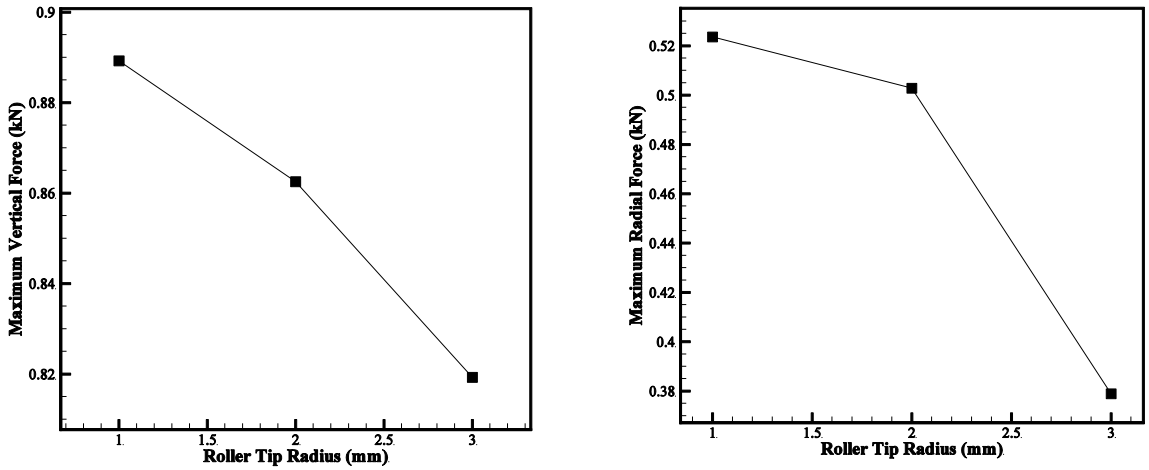

a- Vertical b- Radial

Maximum a- vertical and b- radial forces exerted on the roller for different radius of tips of roller

Table 1: The chemical compounds according to the data from Jia et al. [24].

Alloys	**Zn**	**Mn**	**Cu**	**Fe**	**Si**
percent	0.05	0.025	0.125	0.25	0.225

Table 2: all constant values of equation (1)

m9	m8	m7	m5	m4	m3	m2	m1	A
0	0	0	0	44	0.019	0.22	21	161.96

Table 3: Different calculated parameters and compared in three methods

	Exp. Data [24]	Forge3D results [24]		Present work	
Direction (°)	Final Straight Length (m)	Final Straight Length (m)	$\sqrt{R^2}$	Final Straight Length (m)	$\sqrt{R^2}$
0	77.2	77.7	99.35	77.4	99.74
90	78.3	79	99.11	77.9	99.49
180	77.5	78.3	99	77.8	99.61
270	77.4	78.5	98.6	77.2	99.74